EUROFUSION WPPFC-PR(14) 12681

K. Dobes et al.

Interaction Dynamics of Beryllium Surfaces with Nitrogen and Deuterium Projectiles

Preprint of Paper to be submitted for publication in
New Journal of Physics

This work has been carried out within the framework of the EUROfusion Consortium and has received funding from the Euratom research and training programme 2014-2018 under grant agreement No 633053. The views and opinions expressed herein do not necessarily reflect those of the European Commission.

Interaction Dynamics of Beryllium Surfaces with Nitrogen and Deuterium Projectiles

Katharina Dobes[1], Martin Köppen[2], Martin Oberkofler[3], Cristian P. Lungu[4], Corneliu Porosnicu[4], Christian Linsmeier[2], and Friedrich Aumayr[1]*

[1] Institute of Applied Physics, TU Wien, Wiedner Hauptstraße 8-10, 1040 Vienna, Austria
[2] Forschungszentrum Jülich GmbH, Institut für Energie- und Klimaforschung – Plasmaphysik, 52425 Jülich, Germany
[3] Max-Planck Institut für Plasmaphysik, Boltzmannstraße 2, D-85748 Garching, Germany
[4] National Institute for Laser, Plasma and Radiation Physics, 077125 Bucharest, Romania

Abstract

The interaction dynamics of beryllium surfaces with mono-energetic nitrogen and deuterium projectiles at keV energies is studied in real time and in situ under controlled laboratory conditions using a highly sensitive quartz crystal microbalance technique. A pronounced fluence dependence is observed for all investigated target-projectile combinations pointing to the formation of mixed material layers for both projectile species. Based on the experimental data and with the aid of TRIDYN simulations, the contribution of individual interaction processes and their dependence on the projectile concentration in the surface can be determined in a unique way. The overall retained projectile fluence is investigated with post mortem nuclear reaction analysis.

For the impact of nitrogen projectiles, the interaction is at first dominated by a projectile implantation. Upon reaching the nitrogen saturation concentration, a transition to dominant surface erosion is found. Steady state conditions are only reached after a cumulative fluence of $\sim 83 \cdot 10^{16}$ N per cm^2, with a steady state sputtering yield of 0.4 beryllium atoms per impinging N. Furthermore, the influence of the nitrogen content in the surface on its oxidation behavior is furthermore investigated.

The influence of such nitrogen containing mixed beryllium layers on the saturation dynamics of deuterium projectiles is investigated by performing experiments with a previously nitrogen-saturated and an as-received, pure beryllium surface. On a nitrogen saturated surface the initial retention probability is higher than on pure beryllium. The deuterium implantation

saturates at a comparable fluence on the two surfaces. For pure beryllium dynamic equilibrium conditions are reached at twice the fluence that is needed to establish a steady state surface composition for the nitrogen-saturated sample. In addition, the deuterium release dynamics upon interrupting surface irradiation is investigated at an elevated surface temperature for both, nitrogen-saturated as well as pure beryllium. It is found that initially the reaction kinetics of the two surfaces is dissimilar, but coincides for longer waiting times.

Keywords: plasma wall interaction, beryllium, erosion, retention, sputtering

* aumayr@iap.tuwien.ac.at

1. Introduction

The largest part of the vacuum vessel wall of the fusion experimental reactor ITER will be covered by beryllium [1]. Beryllium is chosen as a plasma-facing material in fusion research primarily due to its low atomic number Z (for a detailed review on beryllium as a plasma-facing component in fusion devices see eg. [2]). In contrast to e.g. tungsten, the energy loss from the plasma by radiating beryllium species is comparably small and hence the maximum tolerable beryllium concentration in the plasma core is of the order of several percent [3] compared to only about 10^{-5} for tungsten [4]. In addition, beryllium is an excellent oxygen getter material and will thereby aid in improving the vacuum conditions in the fusion reactor vessel.

As carbon is increasingly replaced as a plasma-facing component in today's fusion experiments, the benign cooling effect of intrinsic carbon impurities by radiative power dissipation in the divertor region and the plasma edge is being dismissed [5]. To keep the heat load to the plasma-facing components below the maximum acceptable limit and in order to maintain the radiated power fraction in high power discharges, it will be necessary to introduce artificial seeding impurities into the plasma edge of all-metal fusion machines [6, 7]. Among such seeding gases, nitrogen is strongly favored due to its comparably high radiative characteristics at low electron temperatures [8], which is responsible for its capability of replacing the radiating carbon species in the divertor region of the tokamak. Nitrogen seeding is already successfully implemented in today's fusion experiments such as ASDEX Upgrade [5] and JET [9, 10, 11, 12].

With the introduction of nitrogen into the fusion plasma vessel, the formation of nitrogen containing mixed material layers is expected [13]. Dynamic implantation of nitrogen into the vessel walls or co-deposition with eroded species will result in a modification of the surface structure and the composition of plasma-facing materials during the operation of a fusion reactor [14, 15]. For the interaction of beryllium surfaces with energetic nitrogen projectiles, the formation of a beryllium nitride phase within the ion penetration depth was observed by Oberkofler and co-workers [15]. It is reported that the amount of retained nitrogen increases with applied nitrogen fluence and saturates after a fluence which is in accordance with a surface recession of the order of the

projectile range in the surface. In X-ray photoelectron spectra (XPS) of the surface, the appearance of a nitride peak is observed, while at the same time the metallic beryllium Be 1s peak is increasingly attenuated with the nitrogen content in the surface [15]. The integrated atomic nitrogen fraction of the corresponding XPS peaks points to the formation of a stoichiometric Be_3N_2 compound within the ion range in the surface.

The formation of such mixed material layers can have a severe influence on their surface properties. Important questions that arise in this context are for example how the composition of the first wall in a fusion reactor affects the component lifetimes by altering e.g. the surface erosion yields or their melting point. In addition, the formation of nitrogen containing surface compounds can also have an influence on the retention and recycling behavior of fuelling species (deuterium, tritium).

In this work the saturation dynamics of beryllium surfaces under both, nitrogen and deuterium impact is investigated under controlled laboratory conditions using mono-energetic ion beams. A unique real time insight into the transient saturation dynamics of the beryllium surfaces is obtained using a highly sensitive quartz crystal microbalance technique [16, 17, 18]. From the total mass change rate observed in the experiment, the influence of basic mechanisms (e.g. implantation, sputtering) involved in the build-up of mixed nitrogen as well as deuterium containing beryllium layers can be assessed.

After a brief overview of the experimental setup (section 2) detailed investigations on the interaction of nitrogen ions with a beryllium surface are presented in section 3 (preliminary results have already been published in [19]). Apart from the transient saturation behavior of the beryllium surface under nitrogen impact, erosion under dynamic equilibrium conditions is also investigated. Additionally, the influence of the nitrogen saturation level on the oxidation behavior of the surface is studied.

In the second part of this publication (section 4) results from real time studies of the dynamics of deuterium retention in beryllium are presented. The influence of the presence of implanted nitrogen on the retention behavior is assessed by comparing results from clean, as-received samples with previously nitrogen-saturated surfaces.

2. Experimental Approach

The Quartz Crystal Microbalance Setup

Total mass change rates of beryllium surfaces are studied using a highly sensitive quartz crystal microbalance (QCM) technique developed at TU Wien [16, 17, 18]. The mass sensitive part of the setup is a stress compensated cut quartz crystal, which is driven at its thickness shear mode in series resonance at a resonance frequency of ~ 6 MHz. One side of the quartz is coated with a 500 nm thick beryllium layer. The beryllium surfaces are fabricated by thermionic vacuum arc deposition at the National Institute of Laser, Plasma and Radiation Physics in Bucharest [20]. They are transferred in air before being installed in the vacuum chamber for ion beam exposure. The beryllium samples used in the present studies therefore all exhibit a native oxide layer on the surface.

The relative mass change of the target film is determined from the change in the resonance frequency of the quartz crystal according to the relation $\Delta f/f = -\Delta m/m$ [21]. From this the mass change rate $\Delta m/\Delta\Phi$ [amu per projectile] can be calculated if the impinging ion current density is known. By integration, the cumulative mass change of the surface under ion beam exposure can be identified, i.e. $\Delta m = \int_0^{\Phi'} \Delta m/\Delta\Phi \cdot d\Phi$ [amu per cm^2]. In our experiments, the mass change rate is thus determined from the slope of a linear fit to the frequency-change curve with applied fluence. In cases where this rate changes with the cumulative ion fluence, a stepwise linear approximation is used to evaluate the mass change rate. It shall be stressed here, that the QCM technique is by design only capable of detecting total mass changes, i.e. the balance of any mass loss due to e.g. erosion and mass increase due to e.g. projectile implantation. Additionally, no information on the actually sputtered species is delivered.

The quartz crystal is mounted on a sample holder in an ultra high vacuum (UHV) chamber at a base pressure of approximately ~ $1 \cdot 10^{-9}$ mbar. The holder is equipped with a Faraday cup for frequent ion current density measurements in between ion beam exposures of the surface. A linear translation stage allows for

changing between quartz and Faraday cup positions in the UHV chamber. Both during ion beam exposure as well as between individual measurements, the surface temperature is kept at 465 K, which is expected to be a typical ITER first wall temperature [22]. In addition, at this temperature the resonance frequency of the quartz is least sensitive to temperature fluctuations and any influence of temperature changes resulting from the ion beam impact are minimized. The sensitivity of the QCM setup is in the order of 0.2 amu/ion·μA/cm^2 [17, 18], which corresponds to approximately $5 \cdot 10^{-5}$ beryllium monolayers per second or $3 \cdot 10^{-6}$ amu per ion for typical ion current densities characteristic to the experimental conditions in the presented investigations (i.e. of the order of some tens of μA per m^2 or $\sim 10^{13}$ atoms per cm^2 and second).

The beryllium surfaces are exposed to an ion beam of either molecular nitrogen N_2^+ or deuterium D_2^+. The ion beam is produced in a commercial electron impact ion source (SPECS IQE 12/38), which is equipped with a Wien filter for mass separation. To investigate the saturation dynamics, the projectile ions are accelerated from the ion source with a voltage of 5000 V, which result in a surface impact energy of 2500 eV per constituent nitrogen or deuterium atom. By means of two lenses and a pair of deflection plates the extracted ion beam is guided and focused onto the sample position in the experimental chamber. A pair of deflection plates at the end of the ion source is supplied with two AC voltages of different frequency in order to rapidly scan the ion beam across the whole active area of the crystal (i.e. an area exceeding 7 x 7 mm^2). By this, the ion beam density covering the sample area is held constant and can be determined accurately. In addition, any mechanical stress imposed on the crystal by non-uniform erosion is avoided. For a more detailed description of the QCM setup see e.g. [17, 18, 19, 23].

After ion beam exposure, the total amount of retained nitrogen and deuterium projectiles is determined using non-resonant nuclear reaction analysis (NRA). These measurements are conducted with the tandem accelerator located at IPP Garching, exploiting the D(^{3}He, p)^{4}He and the ^{14}N(^{4}He, p)^{17}O reaction with 2.00 MeV ^{3}He$^+$ and 4.94 MeV ^{4}He$^+$ ions, respectively.

The experimental results obtained in our studies are compared to computer simulations using the TRIDYN-FZR simulation package and SDTRIM.SP [24, 25,

26] (in the following referred to as 'TRIDYN' for simplicity), which is a Monte Carlo Code approximating the particle – substrate interactions by a series of binary collisions and accounting for dynamic compositional changes of the surface as a result of high fluence particle irradiation. The simulations are used to verify the experimental findings and to elucidate the individual contributions of the interaction mechanisms involved in the saturation dynamics of the beryllium surface under N and D impact.

3. Transient and Steady State Sputtering of Beryllium by Nitrogen

3.1 Nitrogen Saturation

The transient saturation behavior of a beryllium surface under nitrogen impact is determined for the impact of N_2^+ projectiles at an energy of 2500 eV per nitrogen atom (i.e. 5000 eV per molecular projectile). The impinging ion flux is kept constant throughout the entire surface irradiation, at approximately $\sim 2 \cdot 10^{13}$ nitrogen atoms per cm^2 and second.

To estimate the range of the nitrogen projectiles in a clean beryllium surface, a static TRIDYN simulation is conducted in which any implantation of projectiles is suppressed. In Figure 1 the fraction of stopped projectiles as a function of the

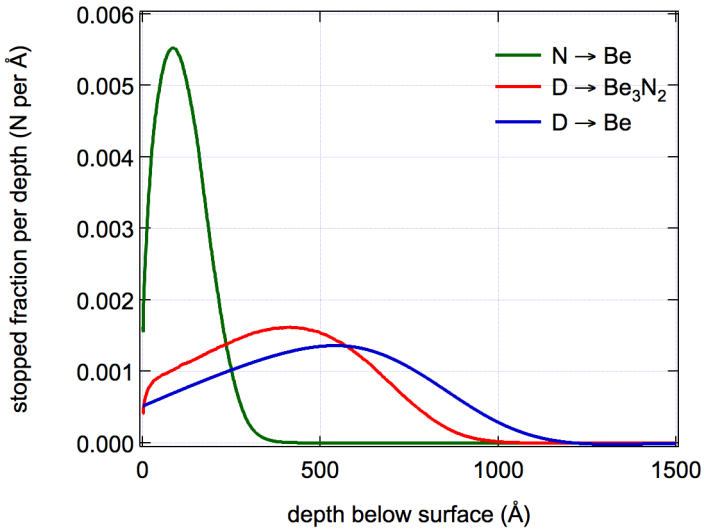

Figure 1: Comparison of the fraction of stopped projectiles according to TRIDYN for all investigated target - projectile combinations (N on beryllium, D on beryllium, D on beryllium nitride) at 2500 eV impact energy. From the maximum of these implantation profiles, the projectile ranges, i.e. the most probable implantation depths can be estimated. They are ~ 87 Å for N in Be, ~ 542 Å for D in Be and ~ 415 Å for D in Be_3N_2.

depth below the surface is shown (in green). For the subsequent deuterium implantation experiments (see section 4), corresponding implantation profiles for deuterium in stoichiometric beryllium nitride (red) and in beryllium (blue) are also shown for comparison.

The maximum of the nitrogen implantation profile, i.e. the most probable implantation depth, lies at about 87 Å below the surface. As nitrogen projectiles are not observed to diffuse much beyond their implantation zone in a beryllium surface [15], it can be expected that first a nitrogen concentration profile builds up in the surface, which is based on the implantation profile in Figure 1. By continuous surface recession due to erosion and simultaneous implantation of projectiles, this implantation profile will broaden with the applied fluence.

This is also supported by a dynamic TRIDYN simulation for the evolution of the nitrogen concentration with accumulated nitrogen fluence. In Figure 2 results for three surface composition profiles at different cumulative projectile fluences are shown, i.e. for low ($\Phi = 3 \cdot 10^{16}$ N per cm^2), intermediate ($\Phi = 6 \cdot 10^{16}$ N per cm^2) and high flunece ($\Phi = 10 \cdot 10^{16}$ N per cm^2) with respect to the implantation profile.

In the simulation the nitrogen content in the surface is restricted to the

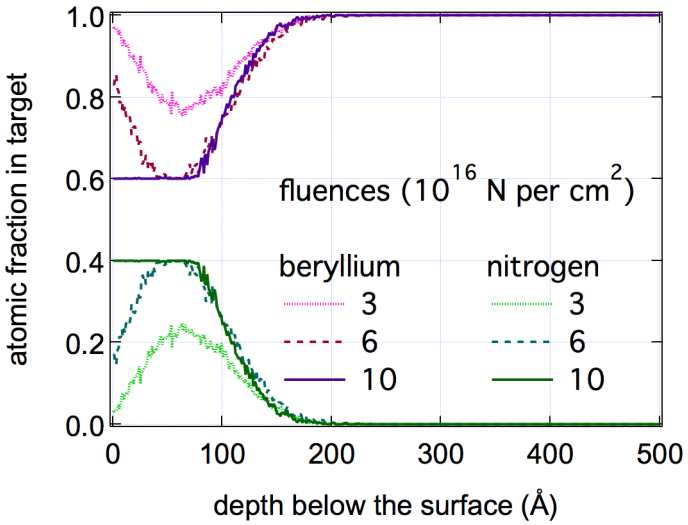

Figure 2: Reults from a TRIDYN simulation for the evolution of the surface composition profiles as a function of the applied nitrogen fluence. The initial implantation profile ($\Phi = 3 \cdot 10^{16}$ N per cm^2) broadens for intermediate fluences ($\Phi = 6 \cdot 10^{16}$ N per cm^2). In steady state a nitrogen saturated surface region is established, which extends from the surface to below the maximum of the initial implantation profile ($\Phi > 10 \cdot 10^{16}$ N per cm^2). The impact energy of the nitrogen projectiles in the simulation is 2500 eV.

stoichiometric concentration in Be_3N_2, i.e. to an atomic fraction of 0.4. The local saturation concentration is first established at the maximum of the implantation profile (cf. profile at $\Phi = 6 \cdot 10^{16}$ N per cm^2 in Figure 2). This saturated surface region then broadens with increasing fluence until steady state conditions are reached and a nitrogen saturated region is established, which extends from the surface to beyond the maximum of the initial implantation profile (cf. profile at $\Phi = 10 \cdot 10^{16}$ N per cm^2 in Figure 2). The thickness of the resulting nitrogen saturated region therefore depends on the projectile impact energy.

In Figure 3 the experimentally observed evolution of the mass change rate $\Delta m/\Delta\Phi$ is shown as a function of the applied fluence of nitrogen atoms. This curve comprises the nitrogen saturation behavior of the beryllium sample from an as-received to a nitrogen saturated surface with a steady state surface composition.

The saturation curve can be devided into four sections [19], as is indicated in Figure 1 by the dashed vertical lines:

① $\Phi \leq 0.4 \cdot 10^{16}$ N/cm^2: an initially very pronounced negative mass change rate, which slows down quickly with increasing fluence.

② $0.4 \cdot 10^{16} \leq \Phi \leq 12 \cdot 10^{16}$ N/cm^2: a regime of positive net mass change rate (i.e. positive $\Delta m/\Delta\Phi$).

③ $12 \cdot 10^{16} \leq \Phi \leq 83 \cdot 10^{16}$ N/cm^2: a regime of negative net mass change

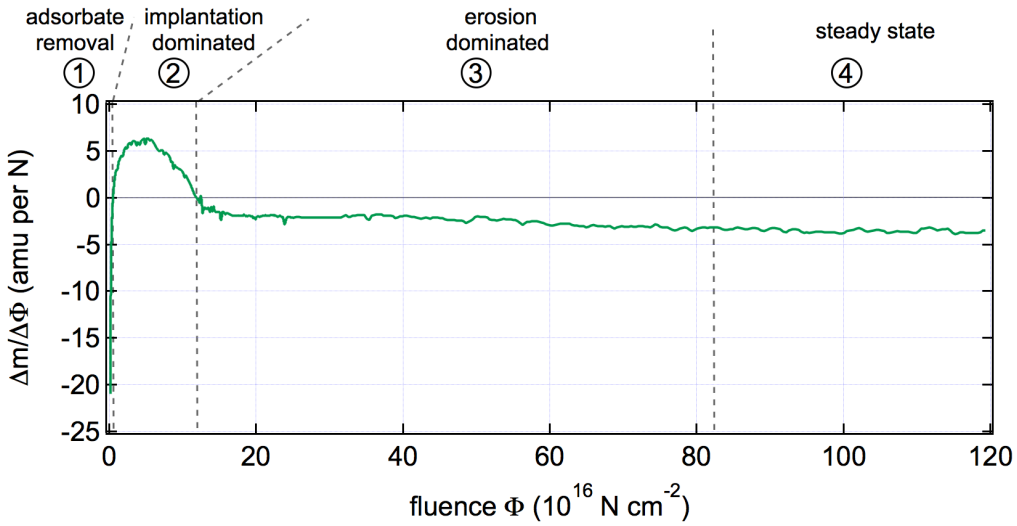

Figure 3: Evolution of the total mass change rate observed when saturating a virgin beryllium surface with nitrogen ions at an impact energy of 2500 eV per atom. Four interaction regimes can be distinguished. For details see text.

rate, where the erosion rate still changes with the ion fluence (i.e. negative $\Delta m/\Delta\Phi$).

④ $\Phi \geq 83 \cdot 10^{16}$ N/cm^2: steady state erosion, where the observed erosion rate remains constant with increasing ion fluence.

The total observed mass change rate represents the balance of different processes which occur simultaneously as the surface is bombarded with nitrogen projectiles: Impinging nitrogen projectiles are implanted according to the implantation profile in Figure 1. They are retained at a depth at which they come to rest in the surface. At the same time material is simultaneously eroded. As sputtered particles predominantly originate from within a rather shallow sub-surface region [27], the implanted nitrogen projectiles will at first not contribute as much to the total sputtering yield. By continuous surface recession due to erosion and simultaneous projectile implantation, the nitrogen concentration profile will eventually broaden while at the same time the nitrogen content at the surface will gradually increase (cf. Figure 2). A dynamic equilibrium of the above processes is established, as soon the composition depth profile becomes constant which results in a saturation of the nitrogen content in the surface. In this case, the observed mass change rate becomes independent of the applied nitrogen fluence.

This interaction scheme is reflected in the four individual interaction regimes indicated in Figure 3, as will be discussed in the following.

① Removal of surface adsorbates ($\boldsymbol{\Phi \leq 0.4 \cdot 10^{16}}$ N/cm^2)

Initially a very efficient mass removal is observed, which decreases rapidly with applied ion fluence. This can be attributed to the removal of surface adsorbates from the fresh, un-irradiated surface.

X-ray photoelectron spectroscopy investigations performed on a virgin beryllium sample suggest that initially the surface is covered by some carbon contamination and a native beryllium oxide layer, originating from the storage of the samples in air between their production and the installation in the experimental UHV chamber.

② Implantation dominated regime ($0.4 \cdot 10^{16} \leq \Phi \leq 12 \cdot 10^{16}$ N/cm²)

Following this initially very efficient mass removal, a regime of net mass increase, i.e. positive mass change rate is observed for a nitrogen fluence ranging from $\Phi \sim 0.4 \cdot 10^{16}$ to $\Phi \sim 12 \cdot 10^{16}$ N per cm² (cf. Figure 3). In the balance of nitrogen implantation (Y_{imp}) and simultaneous surface erosion of both, implanted projectiles and the beryllium substrate (Y_N and Y_{Be}, respectively) the mass increase rate due to implantation in this regime exceeds the total sputtering yield, i.e.:

$$Y_{imp} > Y_{Be} + Y_N$$

It is however not straightforward to disentangle these contributions in the mass change rate observed in the experiment. The evolution of the implantation rate Y_{imp} with increasing fluence will depend on the local nitrogen concentration at the depth, where the projectile comes to rest (cf. Figure 2). Above a certain local saturation concentration (for stoichiometric Be_3N_2 40 at. %), additional nitrogen cannot be retained and effuses out of the surface, which will result in a reduction of Y_{imp}. The evolution of Y_{imp} with applied projectile fluence will therefore be connected to the evolution of the implantation profile. On a fresh, clean surface, the implantation rate should initially exhibit a maximum. As the saturation concentration is reached around the maximum of the implantation profile, Y_{imp} will start to decrease.

In the experimentally observed mass change rate (Figure 3) this is reflected by a relatively broad maximum in the mass change rate around a cumulative fluence of $\Phi \sim 5 \cdot 10^{16}$ N per cm². With increasing fluence the mass change rate is still positive but decreases, as the implantation rate gradually decreases. At a fluence of $12 \cdot 10^{16}$ N per cm² the N implantation is balanced by surface erosion.

A lower estimate for the initial (i.e. maximum) implantation rate Y_{imp}^0 can be deduced from the mass change rate at the maximum in Figure 3, i.e. $Y_{imp}^0 \approx \Delta m/\Delta\Phi\,|_{max} \sim 6$ amu per N (or a fraction of 0.43 incident projectiles being retained in the surface).

In this simple estimate, any simultaneous mass loss due to surface erosion is however neglected and the actual initial implantation rate Y_{imp}^0 will in fact be

higher. A more accurate estimation of Y^0_{imp} should include the total surface erosion rate, i.e. $Y^0_{imp} \approx \Delta m/\Delta\Phi\,|_{max} + Y^0_{Be} + Y^0_N$

In contrast to Y_{imp}, the evolution of the partial sputtering yield of both, implanted nitrogen Y_N and the beryllium substrate Y_{Be} will only depend on the near surface concentrations of the individual species (not on the entire composition profile), as the escape depth of sputtered particles is shallow. For low projectile fluences, the erosion of retained nitrogen does not substantially contribute to the total sputtering yield, which is instead dominated by beryllium sputtering. With increasing nitrogen fluence, nitrogen will also accumulate near the surface (cf. Figure 2), which will lead to an increase in Y_N, and simultaneously reduce the availability of beryllium in the escape zone of sputtered particles. In addition the evolution of the partial sputtering yields of beryllium and nitrogen will also be influenced by differences in the energy distribution to the two surface constituents. In the collision cascade, which is initiated by the impinging projectile, the energy transfer between two colliding particles depends on their reduced mass. This mass effect will result in a higher near surface energy deposition to the nitrogen atoms, thereby favoring the sputtering of nitrogen as compared to beryllium. On the other hand the escape probability of surface atoms also depends on their range in the surface, which is usually larger for lighter particles, i.e. in this case for the beryllium atoms. In addition, differences

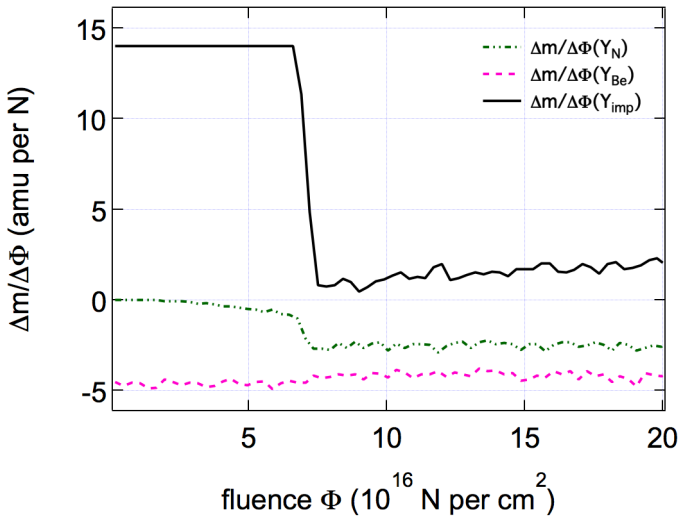

Figure 4: Evolution of the mass change rates for the involved processes (Y_N, Y_{Be}, Y_{imp}) as estimated with TRIDYN. The nitrogen impact energy in the simulation is 2500 eV.

in the chemical bonding of the surface constituents might lead to a preferential sputtering and consequently depletion of the component, which is more weakly bound.

Both, bonding as well as mass effects, are included in the TRIDYN simulation of the collision cascade, which can thus give a better estimate for both, the implantation, as well as the individual sputtering rates. The evolution of all of the involved processes (Y_N, Y_{Be}, Y_{imp}) obtained in the TRIDYN simulation is shown in Figure 4. The simulation predicts that initially, essentially all impinging projectiles are retained. The implantation rate then reduces drastically, as the saturation concentration is being reached at the maximum of the implantation profile, i.e. at a fluence of $\sim 6 \cdot 10^{16}$ N per cm^2 (cf. Figure 2). This fluence is in good agreement with the fluence, at which a reduction of the overall mass increase rate is also observed in the experiment (cf. Figure 3).

For a better estimate of the experimentally observed initial implantation rate Y_{imp}^0, the initial surface erosion rate from this simulation can be added to the mass increase, i.e. $Y_{imp}^0 \approx \Delta m/\Delta\Phi\,|_{max} + Y_{Be}^0 + Y_N^0 \sim 10.7$ amu per N (or a retained projectile fraction of ~ 0.76).

Another approach is to neglect Y_N^0 to a first approximation (cf. Figure 4), and approximate the beryllium sputtering yield Y_{Be}^0 by the mass loss rate observed in steady state, i.e. when finally nitrogen implantation exactly balances nitrogen erosion and the nitrogen surface content does not change anymore. In this case the observed surface erosion rate is solely due to beryllium sputtering, i.e. $Y^\infty \equiv Y_{Be}^\infty$. At this point the near surface region is composed of both nitrogen and beryllium. To account for this, the steady state sputtering yield should be scaled with an appropriate value for the beryllium surface concentration. In accordance with previous investigations [15] for the interaction of nitrogen projectiles with beryllium surfaces, the atomic nitrogen concentration of a stoichiometric beryllium nitride Be_3N_2 compound, i.e. $\Theta_{Be}^\infty \sim 0.6$ can be used. This gives an estimate for the initial implantation rate of $Y_{imp}^0 \sim 82.7\%$. In this approximation any influence of the nitride formation on the beryllium sputtering yield other than the surface dilution (i.e. mass effects on the collision cascade and changes in bonding) is neglected.

③ Erosion dominated regime ($\Phi \gtrsim 12 \cdot 10^{16}$ N/cm²)

Eventually the local nitrogen saturation concentration is reached and additional nitrogen projectiles are implanted less efficiently into the beryllium substrate. Excess nitrogen projectiles are re-emitted from the surface. At some point the erosion of the surface then outbalances the mass increase due to projectile implantation. In the experiment this is reflected by a transition to a regime of net mass removal for fluences ≥ $7.6 \cdot 10^{16}$, which can be seen in Figure 3. This fluence dependency is in principle in good agreement with the TRIDYN simulation (cf. Figure 4).

From the TRIDYN simulation one would however assume that after reaching the local nitrogen saturation concentration, dynamic equilibrium conditions are attained at a fluence of $\sim 10 \cdot 10^{16}$ N per cm². At this point the entire implantation region is saturated with nitrogen (cf. Figure 2) and the retained atomic fraction amounts to approximately 0.15-0.2. As a consequence Y_{Be} decreases slightly from an initial value of $Y_{Be}^{0} \sim$ 4.7 amu per N to $Y_{Be}^{\infty} \sim$ 4.2 amu per N, while Y_N rises from initially zero to $Y_N^{\infty} \sim$ 2.5 amu per N. implantation rate Y_{imp} but also the partial sputtering yields of the involved species (Y_N and Y_{Be}) become constant.

In the experiment, however, it takes much longer until steady state surface conditions are established and the mass change rate becomes constant. While

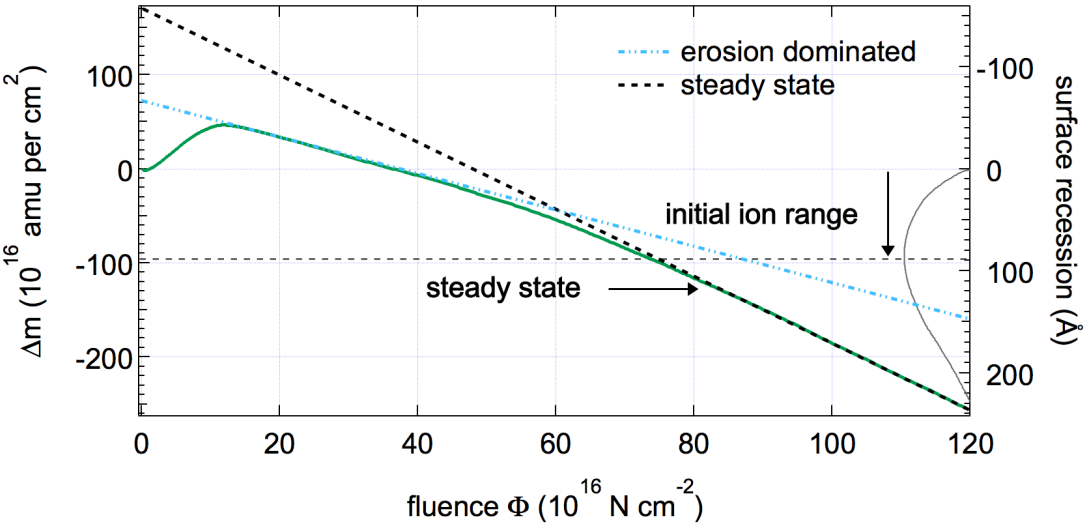

Figure 5: Cumulative mass change Δm and corresponding surface recession during the nitrogen saturation of a beryllium surface as a function of the applied nitrogen fluence at an impact energy of 2500 eV per N. For low fluences the mass change is dominated by projectile implantation. In the sputtering dominate regime, two sections of about constant mass loss are observed (blue and black dashed lines). The initial N implantation profile is also indicated (in grey). For details see text.

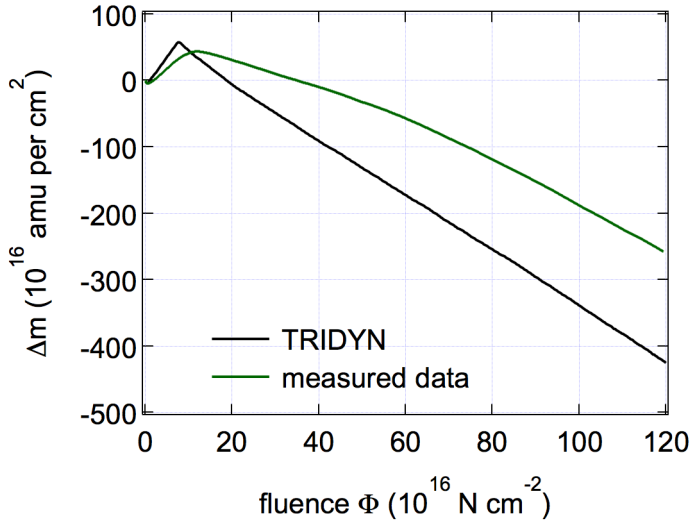

Figure 6: Comparison of the cumulative mass change during N saturation obtained from the experiment (green, see also Figure 3) to results from a TRIDYN simulation (black). The cumulative mass change of the TRIDYN curve incorporates erosion of beryllium and nitrogen species as well as projectile implantation.

this is not so obvious from the trend of the mass change rate in Figure 3 it becomes much more clear when taking a look at the cumulative mass change Δm, i.e. the integrated mass change rate, which is shown in Figure 5.

Although the implantation dominated regime is followed by a regime of about constant mass loss rate, i.e. is proportional to the cumulative mass change (blue dashed fit in Figure 5), this initially constant erosion rate of approximately $Y^{trans} \sim 2$ amu per N is surpassed by a transition region around a fluence of roughly $\sim 60 \cdot 10^{16}$ nitrogen atoms per cm^2. At this point the observed sputtering yield starts to gradually increase again (the measured curve deviates from the linear fit in Figure 5). Steady state surface conditions are finally reached only after a total fluence of $83 \cdot 10^{16}$ nitrogen atoms per cm^2 has been applied to the surface. The observed sputtering yield becomes constant and from this point onwards does not change anymore with increasing ion fluence (black dashed line in Figure 5).

In steady state the number of implanted projectiles exactly balances the number of eroded nitrogen atoms ($Y_{imp} = Y_N$). Therefore, the observed erosion rate arises from beryllium sputtering only, i.e.:

$$Y^{\infty} = Y_{Be}^{\infty} = 0.4 \text{ Be per N}$$

The nature of the two separate regimes of constant sputtering yield is not entirely clear. In Figure 6 the experimentally obtained cumulative mass change (in green, cf. Figure 3) is compared to the cumulative mass change as predicted

by TRIDYN (in black). The TRIDYN curve combines the simulated mass change rates due to projectile implantation and sputtering of all involved species (beryllium as well as nitrogen). The shape of the two curves in Figure 6 is similar, but there are some distinct differences. As stated above, TRIDYN would expect a higher initial nitrogen retention rate (Y_{imp}^{0}), which is reflected in a steeper increase of the cumulative mass change of the TRIDYN curve in the implantation dominated regime at fluences below $\Phi \leq 10 \cdot 10^{16}$ nitrogen atoms per cm^2. After the nitrogen saturation concentration of 40% has been reached in the implantation zone of the surface, TRIDYN predicts a net surface erosion, with a constant erosion rate of in total $Y^{\infty} \sim 0.5$ beryllium atoms per nitrogen atom. In the TRIDYN simulation, the transition to net erosion is promptly followed by achieving steady state surface conditions. In contrast to this, steady state erosion conditions are only reached at a much higher fluence in the experiment (i.e. $\sim 83 \cdot 10^{16}$ N per cm^2). Although the steady state sputtering yield obtained from TRIDYN is very similar to the steady state sputtering yield observed at the end of the experimental curve, the intermediate regime of constant erosion succeeding the implantation dominated regime in the experiment, is not reflected in the simulated data.

As the diffusivity of implanted nitrogen projectiles in the beryllium bulk is expected to be small [15], the nitrogen concentration in the surface will be mostly concentrated around the ion penetration depth of about $\sim$ 87 Å (cf. Figure 1). This is supported by the observation [15] that upon interaction of energetic nitrogen projectiles with a beryllium surface, the thickness of the resulting steady state beryllium nitride layer is of the order of the ion penetration depth. In this case a surface layer as thick as the ion range has to be eroded before the nitrogen-rich mixed material layer emerges to the surface and steady state conditions are obtained. From the cumulative mass loss in Figure 5 and an appropriate value for the surface density, the total surface recession can be estimated. In Figure 5 the cumulative mass change (left axis) is converted into a surface recession (right axis), using a linear interpolation between the density of beryllium, i.e. $\rho_{Be} \sim 1.8$ g/cm^3, and beryllium nitride for higher fluences, i.e. $\rho_{Be_3N_2} \sim 2.7$ g/cm^3. In order to estimate at which point in the nitrogen saturation curve, a surface layer of the order of the ion penetration depth has been eroded,

the most probable range below the initial surface as predicted by TRIDYN is also indicated in Figure 5 by the N implantation profile depicted on the right.

According to this estimation, the experimentally observed surface recession exceeds the most probable ion penetration depth of ~ 87 Å only at a fluence of about $74 \cdot 10^{16}$ nitrogen projectiles per cm^2, i.e. slightly below the fluence that is needed to obtain steady state surface conditions in the experiment. In this case the local nitrogen saturation at the center of the implantation profile (corresponding to the TRIDYN implantation profile at $\Phi = 3 \cdot 10^{16}$ N per cm^2 in Figure 2) might indeed be reflected in the experimental data by the transition from net mass gain to net erosion, as at this point the implantation probability is strongly reduced and the erosion of the surface starts to dominate the observed mass change rate. A considerably higher nitrogen fluence might however be needed until this nitrogen saturated sub-surface zone extends into the first few monolayers, from which sputtered particles originate (cf. implantation profile at $\Phi = 10 \cdot 10^{16}$ N per cm^2 in Figure 2).

The about constant total erosion rate, which is observed in the experiment following local saturation of the nitrogen concentration, i.e. for fluences $20 \cdot 10^{16} \lesssim \Phi \lesssim 40 \cdot 10^{16}$ N per cm^2, suggests an about constant near surface composition. This implies that initially, implanted nitrogen does not contribute much to the total erosion rate as the surface layer from which sputtered particles originate is mainly composed of beryllium. At a fluence of about $40 \cdot 10^{16}$ nitrogen atoms per cm^2 the nitrogen-rich layer finally starts to contribute to the surface erosion and the partial nitrogen sputtering yield gradually increases, which is marked by the observed relatively broad transition region to steady state erosion conditions in Figure 5. Once the surface recession exceeds the initial ion penetration depth, dynamic equilibrium conditions are obtained and the surface composition within the entire ion penetration depth becomes constant.

In this simplified picture the three regimes of interaction regimes observed in the experiment (cf. Figure 3) can then be explained and summarized in the following way: first a predominant nitrogen implantation until local saturation is reached (implantation dominated regime), second a constant erosion rate as the nitrogen saturated sub-surface layer does not yet contribute to erosion (erosion dominated regime) and third steady state conditions at which the nitrogen

saturated layer has finally emerged to the surface and the composition in both, the implantation zone as well as the layer from which sputtered particles originate become constant (steady state).

In the erosion dominated regime, a balance between beryllium sputtering and the steady state nitrogen implantation rate Y_{imp}^{∞} exists, since at the implantation depth the saturation concentration is already reached. With the steady state beryllium sputtering yield Y_{Be}^{∞}, an estimate for Y_{imp}^{∞} is then achieved in the same way as for Y_{imp}^{0}, i.e.

$$Y_{imp}^{\infty} \sim 28.5\%$$

From the TRIDYN simulation a steady state implantation rate of 18 % would be expected.

An alternate explanation for the observed saturation dynamics and especially the two distinct regimes of about constant mass loss rate could be found in the surface morphology. Scanning electron microscopy images of the nitrogen-saturated surface in comparison to an unirradiated sample reveal that the nitrogen exposure results in a roughening of the surface. At normal incidence the sputtering yield will generally increase with surface roughness [28]. Based on the evolution of the mass change rate alone, the transition from the initial erosion dominated regime to steady state sputtering in Figure 5 could reflect both, a change in surface composition as well as an alteration of the surface morphology.

Following the nitrogen saturation of the surface, post mortem non-resonant nuclear reaction analysis (NRA) measurements were performed with helium projectiles at an energy of 4.94 MeV. To estimate the total amount of retained nitrogen, the protons from the reaction $^{14}N(^{4}He,p)^{17}O$ were detected. From the observed reaction rate, the integrated areal density of nitrogen is approximately $14 \cdot 10^{16}$ atoms per cm^2. It is not straightforward to convert this value into an atomic concentration of implanted nitrogen projectiles within the surface, since the thickness to which the nitrogen saturated surface layer is confined, i.e. from which the NRA signal originates, cannot be determined in this experiment. The implantation depth can be estimated based on the implantation profile obtained from TRIDYN (cf. Figure 1). Although the nitrogen range profile in Figure 5 suggests that the nitrogen concentration will peak at a depth of roughly 87 Å, a

significant amount of nitrogen will be implanted beyond this depth and above. In an attempt of making a rough estimation for the nitrogen concentration in the surface, the nitrogen range profile can be cut-off e.g. at 20% of its maximum value, by which it is assumed that a representative integration depth for the observed nuclear reaction is ~ 250 Å. If the integrated areal nitrogen density determined in the NRA measurement is then compared to the density of beryllium nitride, i.e. 0.148 at per $Å^3$ [29], this would imply a nitrogen content of on average $\Theta_N \sim 0.37$ (close to the stoichiometry of Be_3N_2).

3.2 ④ Steady state erosion ($\Phi \geq 83 \cdot 10^{16}$ N/cm^2)

As soon as steady state surface conditions are reached, the interaction of the nitrogen projectiles with the beryllium surface is characterized by a constant erosion yield. To estimate this steady state erosion yield as a function of the projectile impact energy, a nitrogen-saturated surface was bombarded with nitrogen projectiles of varying energy.

The nitrogen-saturated surface was prepared with a total fluence of $120 \cdot 10^{16}$ nitrogen projectiles per cm^2. The sputtering yield of the resulting beryllium nitride surface was determined for normal particle incidence at impact energies in the range of 375 eV per N to a maximum kinetic energy of 2500 eV per N. These measurements were performed without any further treatment or analysis

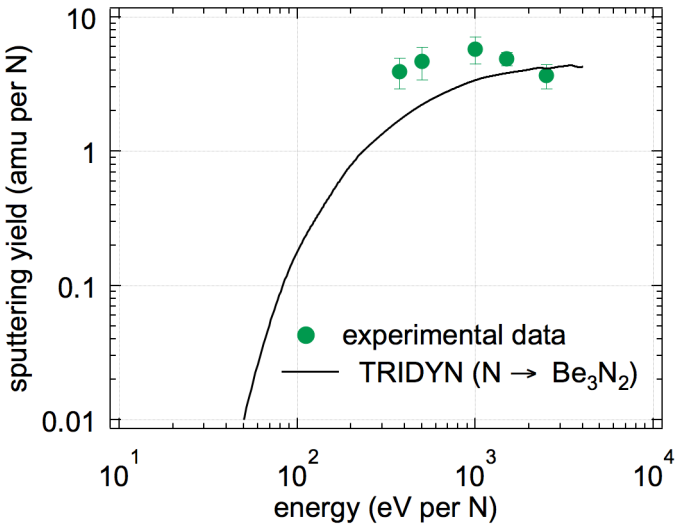

Figure 7: Steady state nitrogen sputtering yield of the nitrogen saturated beryllium surface as a function of the projectile impact energy. Experimental data points (green symbols) are compared to data from a static TRIDYN simulation for sputtering of a Be_3N_2 (black solid line).

of the surface. To keep any projectile induced surface modifications as small as possible for all investigated impact energies, the impact energy of the projectiles and consequently the projectile penetration depth was gradually decreased.

In Figure 7 the experimentally obtained total erosion yields are shown and compared to a static TRIDYN simulation for sputtering of a beryllium nitride Be_3N_2 surface (black solid line). The error bars to the experimental data include the statistical error from a series of consecutive measurements (usually approximately 3) at the same energy and a contribution from variations of the impinging ion current density during surface irradiation as determined from an ion current measurement before and after ion beam exposure.

In the course of the steady state sputtering yield measurements, a total nitrogen fluence of $\sim 9 \cdot 10^{16}$ N per cm^2 was applied to the surface. To check how this might affect the observed yield, the measurement at 2500 eV per N was repeated after the entire series of impact energies had been completed. Within the experimental accuracy of the setup, the sputtering yield observed at the beginning of the series was reproduced.

3.3 Oxidation of beryllium nitride

One of the advantages of using beryllium as a plasma facing material is its affinity to oxygen, which might aid in reducing the impurity concentration in the ITER vessel. When interrupting the nitrogen bombardment in the experiments, indeed a distinct mass increase is at first observed, which can be attributed to the formation a surface oxide from an exposure to the residual oxygen pressure in the vacuum chamber.

Remarkably it is found that the characteristics of the observed oxidation curve strongly depends on the nitrogen saturation level of the surface. When interrupting the nitrogen bombardment at a comparably low cumulative nitrogen fluence, the observed mass increase is much more pronounced than it is for a surface with an almost saturated nitrogen content. This is shown in Figure 8, where two different oxidation curves, i.e. the mass accumulation rate observed right after interrupting the nitrogen bombardment, are compared (mind the different scaling of the ordinates). In the graph to the left the nitrogen

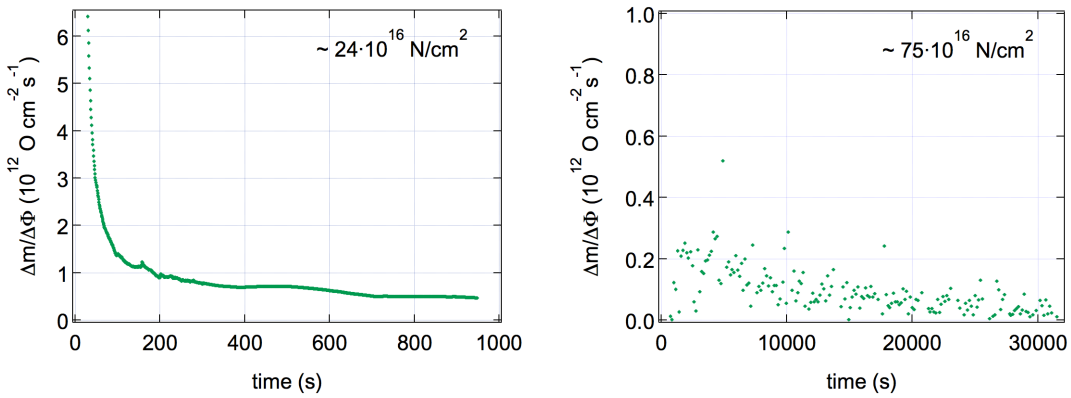

Figure 8: Comparison of the observed surface oxidation for two different nitrogen saturation levels (nitrogen fluences indicated in the insets). The nitrogen irradiation was performed without any intermediate interruption.

bombardment was stopped after a cumulative fluence of $24 \cdot 10^{16}$ nitrogen per cm^2, i.e. during the initial erosion dominated regime of the saturation curve in Figure 5. The curve on the right was obtained during an interruption at a much higher fluence of $75 \cdot 10^{16}$ nitrogen per cm^2, i.e. almost towards steady state surface conditions. In both cases the respective nitrogen fluences were applied without any intermediate interruption. Both oxidation curves were obtained at a comparable residual gas pressure in the low 10^{-9} mbar regime.

With an enthalpy of formation for Be_3N_2 of $\Delta_f H^0 \sim -6.1$ eV per molecule, compared to $\Delta_f H^0 \sim -6.3$ eV per molecule for BeO [30], the formation of beryllium nitride is energetically only a little less favorable than surface oxidation. From the experimentally observed oxidation behavior it seems as if the formation of beryllium nitride on top of the beryllium substrate effectively passivates the surface towards oxidation.

The clear difference in the two oxidation curves shown in Figure 8 also implies that at a fluence of $24 \cdot 10^{16}$ nitrogen atoms per cm^2 (left graph), the nitrogen saturation level at the surface is lower than after a cumulative fluence of $75 \cdot 10^{16}$ nitrogen per cm^2 (right graph). This strongly suggests that during the initial part of the erosion dominated regime, where a constant erosion rate is first observed (i.e. at fluences $20 \cdot 10^{16} \lesssim \Phi \lesssim 40 \cdot 10^{16}$), the nitrogen content at the surface has not yet saturated. The two individual regimes of constant erosion yield in the saturation dynamics of the surface therefore have to be at least partially linked to the evolution of the nitrogen concentration at the surface.

If the nitrogen bombardment is repeatedly interrupted during the saturation of the surface, the passivation towards oxidation is apparently retarded by an intermediate formation of an oxide layer, which then has to be removed again upon resuming the exposure to nitrogen projectiles. The erosion of this oxide layer is marked by an elevated surface sputtering yield compared to the mass loss rate of the underlying beryllium bulk.

4. Interaction of Deuterium with Beryllium-Nitride and Beryllium

As demonstrated in the previous section, the introduction of nitrogen into the vacuum vessel of ITER will result in the formation of nitrogen containing beryllium mixed material layers. An important question that arises in this context is whether the resulting surface compound will have an influence on the fuel retention and recycling behavior of the ITER first wall.

In general it is observed (e.g [31, 32, 33, 34] and references therein) that hydrogen isotope retention is influenced by material parameters such as the diffusivity and the hydrogen solubility, but also depends on the specific material type and the availability of defects, which can serve as trapping sites for implanted hydrogen isotopes [35, 36]. In ITER radiation damage due to neutron bombardment will therefore have a severe influence on the amount of retained fuel in the wall materials [33]. Lattice displacements introduced by the impact of energetic particles such as nitrogen impurity ions may serve as an additional precursor for hydrogen isotope trapping.

Oberkofler and Linsmeier [15] observed that for low deuterium fluences, the retained deuterium projectile fraction is slightly reduced in nitrogen-saturated surfaces compared to pure beryllium. They attribute this to an increased reflection rate of deuterium projectiles by the heavier nitrogen atoms in the surface as compared to the beryllium substrate. At high fluences however, the authors report that the amount of retained deuterium is overall not affected by the presence of nitrogen. For disordered, i.e. not-annealed surfaces, they find that implanted deuterium is released at noticeably different surface temperatures, which they ascribe to a reduced diffusivity of deuterium through the disordered beryllium nitride layer.

For the general retention mechanisms of deuterium projectiles in pure beryllium surfaces it is found that at low fluences, essentially all deuterium is retained [37, 38]. At fluences of about ~ $10 \cdot 10^{16}$ deuterium per cm^2, the deuterium content in the surface usually starts to saturate. By means of temperature programmed desorption (TPD) it could be shown that below this fluence, implanted deuterium is mainly bound to defects in the surface, which are either intrinsically present or induced by preceding projectile impact [37, 39, 40, 41, 15]. Beyond this local saturation concentration fluence of ~$10 \cdot 10^{16}$ D per cm^2, all available defect sites are occupied and additional deuterium is retained in supersaturated binding sites [42]. This is usually accompanied by structural surface changes, like the formation of bubbles, which are filled with molecular D_2 [44] and generally a porous structure in the implantation zone [33]. At elevated surface temperatures above ~ 440 – 470 K (which corresponds to the sample temperature in the present study), these binding sites cannot be occupied [39, 44]. Instead deuterium above the bulk saturation concentration is retained at sites, which can be attributed to a thermally activated formation of beryllium-hydride or hydroxide within the implantation zone or at the surface.

The deuterium saturation concentration within the saturation zone is found to be of the order of D/Be~ 0.35-0.4 [15, 38]. The overall inventory and the exact fluence at which saturation is observed, depend on the projectile energy, i.e. the projectile range in the surface.

In the following real-time studies on the dynamics of deuterium retention in beryllium will be presented. The influence of the presence of implanted nitrogen projectiles on the retention behavior of the beryllium surface is studied by performing comparable experiments on clean, as-received beryllium and on a nitrogen-saturated beryllium surface. The nitrogen-saturated beryllium surface is prepared by applying ~ $100 \cdot 10^{16}$ N per cm^2 at an impact energy of 2500 eV per N, which results in steady state surface conditions (cf. section 3) for continuous N bombardment. The thus established surface is used for the subsequent investigations without further treatment (like e.g. annealing) or breaking the vacuum.

To investigate the deuterium saturation dynamics, molecular D_2^+ ions are used at the same surface impact energy of 5000 eV (i.e. 2500 eV per D). It can be

expected that the majority of the deuterium projectiles will penetrate the nitride layer, and will only be implanted in the underlying beryllium bulk. A static TRIDYN simulation of the respective implantation profiles shows that the most probable implantation depth for deuterium projectiles at this energy is 542 Å in pure beryllium and 415 Å in stoichiometric Be_3N_2 (cf. Figure 1), which both lie much beyond the maximum of the nitrogen implantation profile at 87 Å.

Both during N and D bombardment as well as in between, the surface temperature is kept at 460 K. At this temperature it is anticipated that deuterium will continuously desorb, as it coincides with a deuterium release peak usually observed in TPD [39].

4.1 Deuterium Saturation

On an as-received and a previously nitrogen saturated beryllium surface, the saturation behavior for the impact of 2500 eV per D molecular deuterium ions were studied. The observed cumulative mass change as a function of the deuterium fluence and the elapsed time is shown in Figure 9 for both, the beryllium nitride surface (in blue) and the beryllium sample (in red). The ion flux to the surface was kept constant in both cases, but differed slightly (i.e. $4.6 \cdot 10^{13}$ D per cm^2 and second on the pure beryllium surface, $4.3 \cdot 10^{13}$ D per cm^2 and second on the beryllium-nitride surface). To account for this and to make the two curves in Figure 9 actually comparable, the saturation dynamics obtained on beryllium-nitride was scaled by a factor of $4.3/4.6 \sim 0.93$. Thus the fluence axis (top) corresponds to the saturation dynamics observed on pure beryllium but matches the scaling of the curve obtained on nitrogen-saturated beryllium.

As the fluence, which is required to establish steady state surface conditions under deuterium impact, was rather high, both saturation curves in Figure 9 were recorded in two consecutive measurements, interrupted by an intermediate break. This is indicated in Figure 9 by the shaded areas. During the entire interruption a continuous cumulative mass decrease could be observed, which can be ascribed to thermal desorption of implanted deuterium, as the surface temperature of 460 K corresponds to a deuterium desorption peak usually observed in TPD [39].

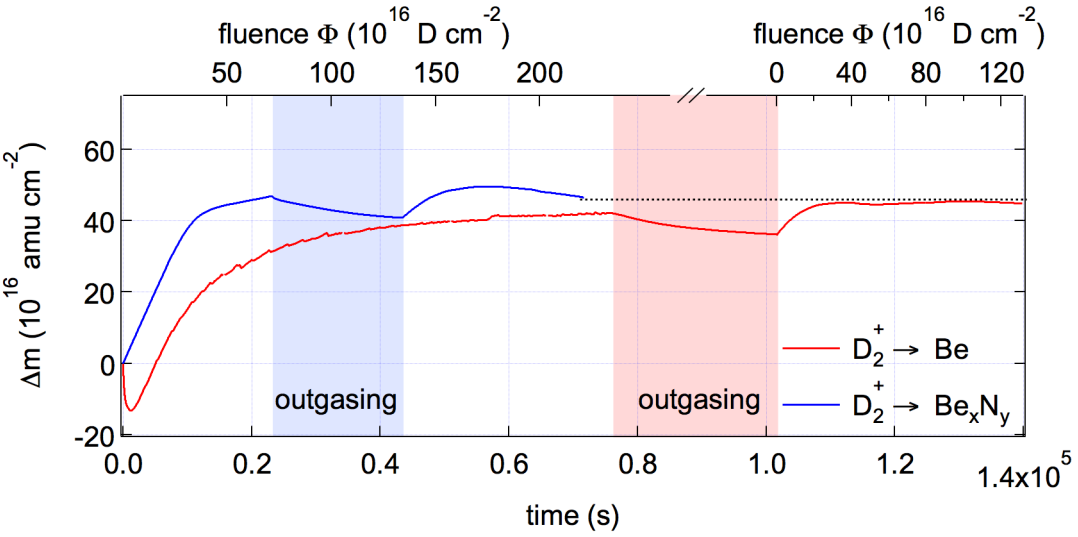

Figure 9: Cumulative mass change Δm during deuterium saturation of a beryllium surface (in red) and a saturated beryllium nitride surface (in blue) as a function of elapsed time and fluence, respectively. For comparability, the curve obtained on Be_xN_y is scaled according to the slightly different projectile fluxes in the two measurements. The shaded areas indicate intermediate interruptions of the D irradiation. For details see text.

The continuous mass loss observed when interrupting the surface irradiation also implies that the second part of the deuterium saturation curves cannot be considered to be a smooth continuation of the mass change rate observed prior to interrupting the deuterium beam exposure. This is indeed reflected in the discrepancy of the trend of the sub-curves before and after interrupting the deuterium irradiation. The indicated fluences of the two consecutive deuterium irradiations (top axis) are therefore not added to a combined total fluence.

In an attempt of merging the two sub-parts of the individual deuterium saturation curves, the effective cumulative deuterium fluence for the second part of the entire deuterium irradiation can be determined by correcting the total fluence (first and second irradiation combined) by a value corresponding to the deuterium fluence overall released during the intermediate interruption. By this it is attempted to correct for the continuous release of implanted projectiles during the interruption, as it results in a reduction of the deuterium content in the surface. In doing so it is assumed that the cumulative mass change observed when ceasing the deuterium irradiation is solely due to desorption, i.e. any simultaneous processes resulting in a (counteractive) cumulative mass change such as e.g. surface oxidation are neglected. On a nitrogen-saturated surface, the oxidation rate is however expected to be small (cf. section 3.3) and this effect is probably negligible. For pure beryllium on the other hand, a pronounced surface

oxidation can be expected. In this case the effective nitrogen fluence estimated in the above-described way might therefore constitute an underestimation of the total deuterium amount actually released during the interruption.

In addition the surface composition might also be changed due to e.g. diffusion of implanted deuterium beyond the implantation zone, which is not taken into account here either.

In Figure 10 the resulting total mass change rate for both nitrogen-saturated (left) and pure (right) beryllium is shown as a function of the thus obtained 'effective' deuterium fluence applied to the surface.

On nitrogen-saturated beryllium, the two sub-parts of the deuterium saturation curve obviously connect very nicely. Still, the observed curve trend upon resuming the deuterium irradiation (light blue) is slightly different at first compared to before the interruption (dark blue). The reason for this might be that processes like surface oxidation or deuterium diffusion do indeed have some influence on the evolution of the surface during the interruption.

On pure beryllium it seems as if the deuterium fluence applied in the second sub-part of the measurement just suffices to balance the intermediately desorbed deuterium amount. The somewhat more pronounced difference in the mass change rate when resuming the deuterium irradiation of the pure beryllium surface, might underpin that a change in the surface composition plays a more important role here compared to the nitrogen saturated surface.

It is generally not straightforward to estimate the rates of all the processes that are involved in the deuterium saturation dynamics of the two surfaces as shown in Figure 9. In comparison with the nitrogen saturation dynamics (cf. section 3), the total mass change rate found under deuterium irradiation is an even more complex superposition of a variety of different processes. Apart from erosion of the involved species, i.e. of beryllium (Y_{Be}) but also implanted deuterium (Y_D) and in the case of the nitrogen-saturated surface nitrogen (Y_N), deuterium projectiles are simultaneously implanted (Y_{imp}). In addition at a surface temperature of 460 K, retained deuterium projectiles are continuously desorbed from the surface (Y_{des}). In the observed mass change rate these processes are all superimposed. The respective rates depend on the concentration of the related species and will therefore change with the applied deuterium fluence.

At first glance the shape of the two saturation curves in Figure 9 seem in principle similar. In contrast to the nitrogen-saturated surface, the deuterium saturation curve on pure beryllium is at first marked by a pronounced cumulative mass removal. This can be attributed to the removal of loosely bound surface contaminants (such as carbon), which for the nitrogen-saturated surface have already been removed in the preceding nitrogen bombardment (cf. Figure 3).

Following this, for fluences below $\Phi \lesssim 25 \cdot 10^{16}$ D per cm^2, the interaction for both investigated surfaces is then marked by a net mass increase rate which is constant with fluence pointing to predominant deuterium retention with a constant retention probability (cf. Figure 9 and Figure 10).

A lower estimate for the initial deuterium retention rate (i.e. deuterium implantation and desorption rate combined, $Y^0_{ret} = Y^0_{imp} - Y^0_{des}$) can be deduced from the slope of the saturation dynamics in Figure 9. On nitrogen-saturated beryllium, the deuterium retention rate is estimated to be $Y^0_{ret}(Be_xN_y) \geq 1.3$ amu per D (i.e. 65%), if to a first approximation simultaneous deuterium desorption and mass removal due to surface erosion are neglected. In a more rigorous approach, a suitable estimate for the erosion yield can be made based on the erosion rate observed at the end of the saturation curve. At this point deuterium release from the surface (due to either sputtering or desorption) is balanced by implantation. The remaining surface erosion yield is rather small, i.e. $Y^{\infty}_{tot}(Be_xN_y) \sim 0.12$ amu per D. This is also supported by TRIDYN, which estimates a surface erosion yield of stoichiometric beryllium-nitride of (Y_{Be} +

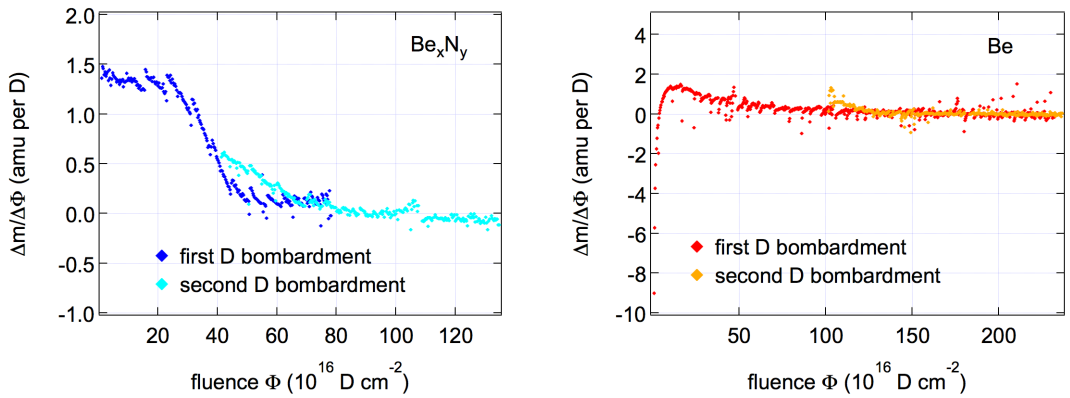

Figure 10: Mass change rate of a nitrogen-saturated (left) and a pure (right) beryllium surface during D saturation. The graphs combine the two consecutive D irradiations by correcting the effective D fluence for the second sub-part by a value corresponding to the total deuterium fluence overall released during the intermediate interruption. For details see text.

Y_N) ~ 0.3 amu per D. Accordingly a more realistic estimate for the overall initial deuterium retention rate on beryllium-nitride is $Y_{ret}^0(Be_xN_y)$ ~ 1.42 amu per D, which corresponds to a probability of ~ 70% of the projectiles being retained in the surface.

On pure beryllium on the other hand the initial slope of the saturation curve in Figure 9 is somewhat smaller, whereas the erosion yield at the end of the curve is negligible. From this it is estimated that the initial retention rate is $Y_{ret}^0(Be)$ ~ 1.15 amu per D or ~58%.

At a fluence of $\Phi \sim 25 \cdot 10^{16}$ D per cm^2, a gradual reduction of the mass increase rate is observed for both surfaces as the deuterium content in the surface apparently starts to saturate. This is in good agreement with observations reported in the literature [15, 38, 39] for reaching the local saturation concentration in the implantation zone at comparable deuterium fluences.

In TPD investigations performed at elevated surface temperatures (above 480 K) Reinelt and co-workers [39] found that for fluences above this local deuterium saturation concentration, deuterium is retained in energetically less favorable binding sites, which can be ascribed to a thermally activated formation of beryllium hydride (SUPERSATURATED?!) [42] or hydroxide. For the beryllium-nitride surface, indeed a second regime of about constant mass change rate is found after the initial retention rate has saturated, for fluences of $25 \cdot 10^{16} \lesssim \Phi \lesssim 80 \cdot 10^{16}$ D per cm^2. The corresponding retention rate in this fluence interval can again be estimated based on the erosion rate observed in steady state. It corresponds to $Y_{ret}^{sat}(Be_xN_y) \sim 0.22$ amu per D (i.e. ~ 11%).

Following these two individual regimes of about constant retention probability, at a fluence of ~ $80 \cdot 10^{16}$ D per cm^2 the observed mass increase rate of the beryllium-nitride surface starts to gradually decline. Finally, at an effective fluence of $\Phi_{eq}(Be_xN_y) \sim 120 \cdot 10^{16}$ D per cm^2 steady state surface conditions are obtained. From this point onwards the surface is gradually eroded with a constant total sputtering yield of $Y_{tot}^{\infty}(Be_xN_y) \sim 0.12$ amu per D. In this case the deuterium content in the surface is in equilibrium, i.e. deuterium release due to thermal desorption and self-sputtering is balanced by the implantation of projectiles.

In contrast to the nitrogen saturated surface, establishing the local saturation concentration is not followed by a second regime of about constant retention rate on pure beryllium. Instead a slow and gradual decrease of the mass increase rate is observed until, after a total effective fluence of $\Phi_{eq}(Be) \sim 230 \cdot 10^{16}$ D per cm^2, steady state conditions are reached. This amounts to about twice the fluence that is needed for establishing dynamic equilibrium when bombarding a nitrogen-saturated surface with deuterium. While for beryllium nitride minor surface erosion was observed, on pure beryllium all involved interaction processes seem to balance each other and the observed mass change rate from this point onwards is virtually zero.

The evolution of the observed mass change rate during deuterium saturation can be compared to a TRIDYN simulation. In the simulation a stoichiometric Be_3N_2 surface compound was assumed to model the nitrogen saturated surface. The maximum deuterium content in the surface was limited to 35% for both investigated surfaces, according to values reported in the literature [15, 39]. The most severe shortcoming of this simulation is its lack of incorporating or reproducing thermally induced desorption of deuterium from the surface and possible chemical reactions like the formation of a beryllium hydride phase.

In Figure 11 the total cumulative mass loss deduced from the measured data (in blue and red) is compared to the total cumulative mass change derived from TRIDYN (in black) for both investigated surfaces. The TRIDYN curve includes erosion of deuterium, beryllium and in case of the nitrogen-saturated surface also nitrogen, as well as projectile implantation.

In the very beginning TRIDYN predicts a cumulative mass change, which is mostly dominated by deuterium implantation with an initial retention rate of 100% for both surfaces. The resulting total cumulative mass change is higher than the cumulative mass increase actually observed in the experiment. Given that thermal desorption of deuterium from the surface is not reproduced by the simulation, this discrepancy, however, is within the expectable limits. According to TRIDYN, the deuterium content in the nitrogen-saturated surface saturates at a fluence of $\Phi_{sat}(Be_xN_y) \sim 60 \cdot 10^{16}$ D per cm^2. In pure beryllium a slightly higher fluence is needed to saturate the surface, i.e. $\Phi_{sat}(Be) \sim 64 \cdot 10^{16}$ D per cm^2. At this point the retention probability is reduced to approximately 5% for

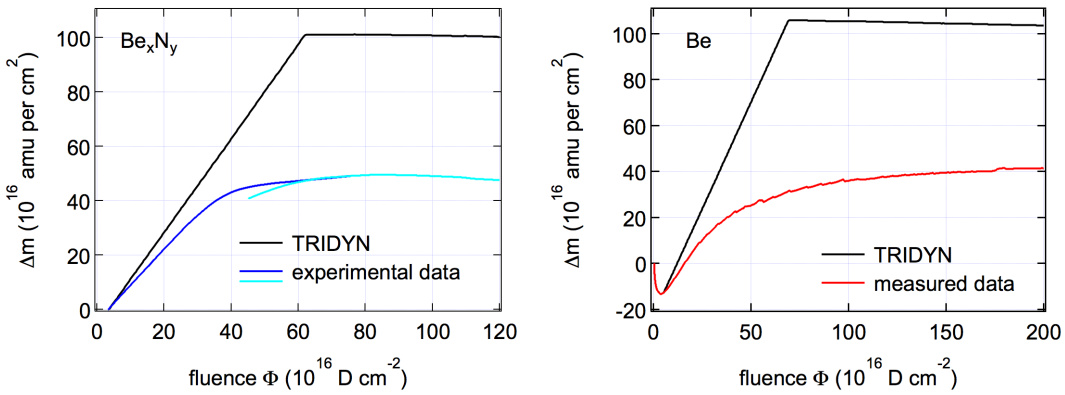

Figure 11: Comparison of the cumulative mass change during D saturation observed in the experiment for Be_xN_y (left) and Be (right) to results from a TRIDYN simulation (black). The cumulative mass change of the TRIDYN curve incorporates erosion of beryllium, nitrogen and deuterium, as well as projectile implantation.

both surfaces and steady state conditions are established. According to TRIDYN, the deuterium bombardment henceforward results in a minor erosion rate of 0.02 amu per D for both, the nitrogen-saturated and the pure surface.

Compared to the experimental data TRIDYN is not capable of reproducing deuterium retention in super-saturation, as it is observed in the experiment. In line with this, steady state conditions are reached only at much higher fluences in the experiment (i.e. $120 \cdot 10^{16}$ D per cm^2 for Be_xN_y and $230 \cdot 10^{16}$ D per cm^2 for pure Be) than predicted by TRIDYN. The simulation agrees with the experiment concerning the fact that higher deuterium fluences are needed to establish the saturation concentration in pure beryllium compared to nitrogen-saturated beryllium, albeit the predicted difference is not as severe as observed in the experiment.

Immediately after the measurement curves in Figure 9 were finished, the samples were removed from the vacuum. Post mortem nuclear reaction analysis was performed with 2 MeV helium projectiles. The areal density of deuterium retained in nitrogen-saturated beryllium was determined to be $\sim 25 \cdot 10^{16}$ D per cm^2, which corresponds to $\sim$ 18% of the effectively applied deuterium fluence (i.e. of the applied D fluence corrected by the total D fluence released during the interruption). On pure beryllium the corresponding nitrogen content is noticeably lower with $17 \cdot 10^{16}$ D per cm^2 being detected. (i.e. ~14 %).

The pronounced discrepancy in the fluence, after which dynamic equilibrium conditions are established on the two surfaces in the experiment, but also the general trend of the observed differences for the deuterium saturation dynamics

can be understood on the basis of some fundamental considerations. The atomic density of pure beryllium ($\rho_{Be} \sim 0.12347$ at per Å^3) is lower than the density of a stoichiometric beryllium-nitride ($\rho_{Be_3N_2} \sim 0.21216$ at per Å^3) [29]. Consequently the expected deuterium ion range is higher in beryllium than it is in beryllium nitride as confirmed by the static TRIDYN simulations displayed in Figure 1. In pure beryllium the deuterium-saturated surface zone will therefore extend further into the bulk than in a nitrogen-saturated surface. From this it could be expected that the total amount of retained deuterium saturates at a higher value for pure beryllium than for the nitrogen-saturated surface. Contrary to this, post mortem nuclear reaction analysis suggests that it is just the other way around: in the beryllium surface the areal density of retained deuterium in steady state is only about 68% of the deuterium amount detected in the nitrogen-saturated surface. In the un-ordered nitrogen-containing surface, lattice displacements induced by the preceding nitrogen bombardment might either serve as additional trapping sites for implanted deuterium or also increase the diffusivity of implanted deuterium. All in all, this effect seems to exceed any differences in the layer thickness of the deuterium-saturated surface zone due to unequal projectile ranges.

	Be_3N_2	**Be**
D range (TRIDYN)	42 nm	54 nm
Atomic density[1]	0.21216 at/Å^3	0.12347 at/Å^3
Y_{ret}^0 (measurement)	0.65 – 0.7	0.58
Φ_{eq} (measurement)	~ 120·10^{16} D/cm^2	~ 230·10^{16} D/cm^2
Y_{tot}^{eq} (measurement)	~0.12 amu/D	~ 0 amu/D
Retained D density (NRA)	~25·10^{16} D/cm^2	~ 17·10^{16} D/cm^2

Table 1: Comparison of the main differences of the deuterium saturation dynamics on the two investigated surfaces. [1] [29].

From a comparison of the mass change rate observed in steady state, the erosion rate of nitrogen-saturated beryllium is apparently a bit higher than for pure beryllium (where essentially no surface erosion is observed in dynamic equilibrium). This is in line with the respective surface binding energies of the two surfaces. Usually the enthalpy of formation is considered to be a suitable measure for the surface binding energy, which is ~4.9 eV/at for beryllium nitride

compared to ~3.4 eV/at for pure beryllium [29].In Table 1 the above comparison is summarized.

4.2 Deuterium Desorption

From the mass change rate observed upon interrupting the deuterium irradiation, the dynamics of the deuterium release can be studied. This was done for both surfaces during the intermediate interruption at deuterium fluences of ~ $78 \cdot 10^{16}$ D per cm^2 in the case of the nitrogen-saturated surface and at ~$230 \cdot 10^{16}$ D per cm^2 for the pure beryllium surface. In Figure 12 the observed mass loss rates are depicted as a function of the time, which elapsed after shutting the deuterium beam off. The data recording was started ~ 400 seconds after interrupting the ion beam exposure.

For the nitrogen-saturated surface (in blue in Figure 12) a pronounced mass loss can be observed during the entire observation interval of almost 30,000 seconds. At first, the detected desorption rate, which corresponds to approximately $2 \cdot 10^{13}$ D per cm^2 and second (estimated by extrapolation to 0 on the time axis), decreases very quickly. After about 3000 s the slowing down of the desorption rate moderates and from this point onwards is not as fast as in the very beginning. It shall be noted here that any surface oxidation will in principle lead to a simultaneous, counteracting mass increase and will therefore result in an underestimation of the observed deuterium desorption rate. However, for the nitrogen-saturated beryllium surface it was found that surface oxidation is suppressed to below any detectable limit (see section 3.3). It is therefore assumed that the surface oxidation rate only plays a minor role in this case.

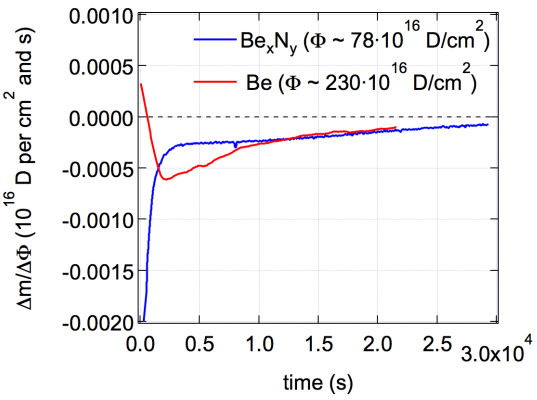

Figure 12: Observed mass change rate of a nitrogen-saturated (in blue) and a pure beryllium (in red) surface as a function of the elapsed time after ceasing the ion irradiation. The cumulative D fluence is $78 \cdot 10^{16}$ D per cm^2 for the nitrogen-saturated, and $230 \cdot 10^{16}$ D per cm^2 for the pure beryllium surface. At the beginning a continuous mass decrease is observed for the nitrogen-saturated surface, which points to outgassing of implanted D. For the pure beryllium surface initially a mass increase is found, which is probably due to surface oxidation. For longer waiting times both curves are dominated by a slowly decreasing D release of similar dimensions.

More detailed information of the initial deuterium release kinetics is contained in the shape of the desorption curve in Figure 12. The amount of released deuterium will be connected to the deuterium content in the surface Θ_D. The actual reaction kinetics depends on the rate-limiting step of the deuterium release process. The initial part of the deuterium desorption curve in Figure 12 can best be fitted according to a second order process, i.e. the desorption rate Y_{des} is proportional to Θ_D^2:

$$Y_{des} = \Gamma_{des} \cdot \Theta_D^2$$

if Γ_{des} is the respective reaction coefficient. In this case the following relation between desorption rate Y_{des} and deuterium surface content Θ_D should apply:

$$\frac{1}{Y_{des}} = \frac{1}{\Gamma_{des}\Theta_D^2} + \frac{2}{\Theta_D} \cdot t + \Gamma_{des} \cdot t^2$$

In Figure 13 a fit (in light blue) of the initially observed inverse desorption rate (in dark blue) according to the above equation is shown. The fact that the initial part of the observed deuterium desorption curve (cf. Figure 13) follows the kinetics of a second order process, implies that the rate limiting step in the desorption of deuterium from the surface requires the presence of two deuterium atoms. In this case the deuterium desorption rate is most likely limited by the D_2 recombination preceding the release from the surface. From the desorption rate observed at this point of the deuterium saturation curve, it can be estimated that about half of the impinging deuterium flux during surface irradiation is re-emitted due to thermal desorption.

For longer observation times (t ≥ 3000 s) the kinetics of the desorption process from the nitrogen-saturated surface clearly changes. This second part of the desorption curve rather follows e.g. a square root dependency, which would indicate that after some time the deuterium desorption rate is limited by deuterium diffusion to the surface.

The corresponding mass change rate of the pure beryllium surface on the other hand looks somewhat different (in red in Figure 12). For the first ~ 600 s a positive mass change rate, i.e. a dominant mass gain of the surface is found. In this case a counteracting, superimposed mass increase apparently outbalances the mass loss due to thermal desorption of implanted deuterium. Most likely this can be attributed to surface oxidation, as pure beryllium is known to readily

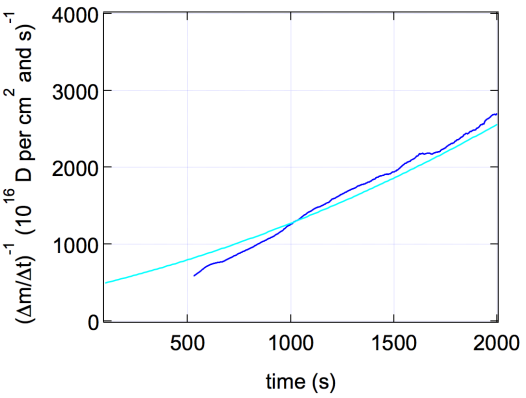

Figure 13: The initial D release curve (dark blue) (cf. Figure 12) can be fitted according to a second order process (light blue), indicating that the observed release rate is limited by D_2 recombination. For details see text.

react with the ambient oxygen. Such a surface oxidation was also observed during the course of the nitrogen saturation, for surfaces where dynamic equilibrium conditions had not been established. Any mass loss rate, which is observed for the pure beryllium surface during the intermediate interruption of ion beam exposure, should therefore only be regarded as lower estimate for the deuterium desorption rate from the surface.

Subsequent to the initially observed dominant mass increase, an overall mass loss is observed, which after approximately 1,500 s even exceeds the desorption rate found for the nitrogen-saturated surface. Similarly, in previous studies [15] a shift of deuterium desorption towards higher surface temperatures was found for Be as compared to Be_xN_y. This was attributed to a reduced diffusivity of deuterium through the disordered nitrogen-containing surface layer as compared to pure beryllium, which retards the release of deuterium from the surface.

After about 11,000 seconds the observed deuterium release rate on beryllium equals the mass change rate found for the nitrogen-saturated surface until the end of the investigated time interval.

5. Summary & Concluding Remarks

The saturation dynamics of a beryllium surface under the impact of energetic nitrogen and deuterium projectiles has been studied in real-time and in situ. In addition the influence of implanted nitrogen projectiles on the saturation

dynamics of deuterium projectiles was investigated by performing comparable deuterium experiments on pure as well as on nitrogen-saturated beryllium. From the saturation curves and supported by TRIDYN, the individual processes contributing to the overall interaction dynamics could be elucidated and their respective rates were successfully estimated.

Under nitrogen impact, the saturation dynamics of the beryllium surface can be subdivided into basically 4 sections: At first a fast removal of loosely bound surface adsorbates is observed. This is followed by an implantation dominated regime ($1 \cdot 10^{16} \leq \Phi \leq 7 \cdot 10^{16}$ N per cm^2), which is marked by a net mass increase and a retention probability of about 76%-86%. At a fluence of $\sim 12 \cdot 10^{16}$ N per cm^2 a transition to dominant surface erosion is observed, which is most likely linked to obtaining the local nitrogen saturation concentration at the projectile implantation depth. The erosion dominated part of the saturation curve is composed of two regimes of about constant mass loss rate, which are separated by a transition region at a fluence of $\sim 40 \cdot 10^{16}$ N per cm^2. Initially a constant erosion yield of ~ 2 amu per N is observed. In steady state ($\Phi \gtrsim 83 \cdot 10^{16}$ N per cm^2) a sputtering yield of ~ 0.4 Be per N is found. While these two regimes are not reflected in TRIDYN simulations, they are still most likely linked to the nitrogen saturation dynamics of the surface. They probably arise from the fact that different N fluences are needed to saturate the surface at the implantation depth (transition from implantation dominated to erosion dominated) and in the near surface escape zone of sputtered particles (transition to steady state). Some influence of a change in surface morphology on the erosion yield cannot be excluded.

Moreover it was found that the oxidation rate of the surface decreases strongly with the nitrogen content in the surface. Towards steady state conditions, the surface oxidation is almost entirely suppressed and the observed mass change rate due to oxidation virtually falls below any detectable limit. A nitrogen saturated surface seems to passivated effectively towards oxidation. Using nitrogen as a seeding gas in ITER might therefore reduce the expected ability of the beryllium first wall to actually getter oxygen.

The dynamics of the deuterium saturation behavior is more difficult to interpret due to the variety of involved processes, ranging from sputtering of Be, N and D to D implantation and thermal desorption of implanted projectiles (as the surface temperature was kept constant at 460 K).

When comparing the saturation dynamics of pure and nitrogen-saturated beryllium, some distinct differences but also similarities are found. For low fluences, an about constant deuterium retention probability is found, which is a bit higher for nitrogen-saturated (~0.7) compared to pure beryllium (~0.58). In the disordered nitrogen-saturated surface, defects introduced by the preceding nitrogen bombardment might serve as binding sites for implanted deuterium and might therefore be responsible for this slightly elevated retention probability. In the environment of a fusion reactor, this might eventually result in a higher overall D retention rate in nitrogen containing, mixed material layers compared to as-received, pure beryllium surfaces. This is also supported by post mortem NRA measurements conducted on both surfaces after steady state surface conditions had been reached, which showed that the amount of retained deuterium is noticeably higher in the nitrogen-saturated compared to the pure beryllium surface.

On both surfaces, the retention rate starts to saturate at a fluence of $\sim 25 \cdot 10^{16}$ D per cm^2, which in analogy to observations reported in the literature [15, 37, 39] can most likely be explained by a local saturation of the deuterium concentration at the ion implantation depth.

Subsequently, the retention dynamics observed for the two surfaces becomes slightly dissimilar. On the nitrogen saturated surface a second regime of about constant retention rate is observed, where the retention probability of deuterium now is ~ 0.11. This second retention regime can most likely be ascribed to a thermally activated retention of deuterium in a beryllium-hydride phase [39] but probably also to the formation of ternary Be-N-D compounds [15]. On the pure beryllium surface on the other hand, establishing the local deuterium saturation concentration is followed by a slow, gradual decrease of the retention rate.

Finally dynamic equilibrium conditions are established for both surfaces, whereas the necessary deuterium fluence is about twice as high for pure

beryllium ($\Phi_{eq}(Be) \sim 230 \cdot 10^{16}$ D per cm^2) than for the nitrogen-saturated surface ($\Phi_{eq}(Be_xN_y) \sim 120 \cdot 10^{16}$ D per cm^2), which is most likely a result of the higher projectile range in pure beryllium compared to stoichiometric beryllium nitride as well as the reduced diffusivity of Be_xN_y. Steady state conditions are marked by a mass change rate of about zero for pure beryllium, i.e. all involved process balance each other. For the nitrogen-saturated surface a constant erosion yield of ~0.12 amu per D is observed.

The deuterium release behavior right after ceasing deuterium bombardment was investigated for both surfaces. On the previously nitrogen saturated surface, overall a net mass loss is observed, implying that the deuterium desorption at least exceeds any surface oxidation (which is expected to be suppressed on nitrogen-saturated beryllium). The desorption kinetics implies that initially the deuterium release rate is limited by D_2 recombination, until eventually other reaction steps such as e.g. deuterium diffusion become rate limiting.

On pure beryllium the desorption dynamics has a markedly different shape. At first a mass increase is observed, which can probably be attributed to dominant surface oxidation. This is followed by a transition to a dominant mass loss, which after ~1500 seconds already exceeds the respective desorption rate observed on nitrogen saturated beryllium. In accordance with previous findings [15] the disordered nitrogen containing surface layer might reduce the deuterium diffusivity towards the surface and by this might retard the deuterium release as compared to pure beryllium. After about some time, the desorption rate from the two surfaces becomes very similar.

Acknowledgements

This work has been carried out within the framework of the EUROfusion Consortium and has received funding from the European Union's Horizon 2020 research and innovation programme under grant agreement number 633053. The views and opinions expressed herein do not necessarily reflect those of the European Commission.

References

[1] ITER Physics Basis Editors, ITER Physics Expert Group Chairs, Co-Chairs, ITER Joint Central Team and Physics Integration Unit, Nucl. Fusion **39** (1999), 2137

[2] G. Federici, R. Doerner, P. Lorenzetto and V. Barabash, in Konings R.J.M., (ed.) Comprehensive Nuclear Mater (ITER Physics Basis Editors, ITER Physics Expert Group Chairs, Co Chairs, ITER Joint Central Team and Physics Integration Unit, 1999)ials for Near-Term Fusion Devices **Vol. 4** (2012), p. 621

[3] H. Bolt, V. Barabash, G. Federici et al., J. Nucl. Mat. **307 – 311** (2002), 43

[4] A. Loarte, G. Saibene, R. Sartori, et al., J. Nucl. Mat. **313 – 316** (2003), 962

[5] A. Kallenbach, R. Dux, M. Mayer et al., Nucl. Fusion **49** (2009), 045007

[6] A. Kallenbach, R. Dux, J. C. Fuchs, et al., Plasma Phys. Control. Fusion **52** (2010), 055002

[7] R. Neu, A. Kallenbach, M. Sertoli et al., J. Nucl. Mat. **415** (2011), S322

[8] A. Kallenbach, M. Balden, R. Dux et al., J. Nucl. Mat. **415** (2011), S19

[9] J. Rapp, N R. de Baar, W. Fundamenski et al., J. Nucl. Mat. **390 – 391** (2009), 238

[10] J. Rapp, Y. Corre, Y. Andrew et al., Nucl. Fusion **49** (2009), 095012

[11] R. Neu, G. Arnouxm M Beurskens et al., Phys. Plasmas **20** (2013), 056111

[12] M. Oberkofler, D. Douai, S. Brezinsek et al., J. Nucl. Mat. **438** (2013), S258

[13] R. P: Doerner, J. Nucl. Mat. **363 – 365** (2007), 32

[14] K. Schmid, A. Manhard, Ch. Linsmeier et al., Nucl. Fusion **50** (2010), 025006

[15] M. Oberkofler and Ch. Linsmeier, Nucl. Fusion **50** (2010), 125001

[16] T. Neidhart, Z. Toth, M. Schmid and P. Varga, Nucl. Instrum. and Meth. B **90** (1994), 496

[17] G. Hayderer, M. Schmid, P. Varga, HP. Winter and F. Aumayr, Rev. Sci. Instrum. **70** (1999), 3696

[18] A. Golczewski, K. Dobes, G. Wachter, M. Schmid and F. Aumayr, Nucl. Instrum. and Meth. B **267** (2009), 695

[19] K. Dobes, M. Köppen, M. Oberkofler, et al., Nucl. Instrum. and Meth. B, (accepted for publication)

[20] C. P. Lungu, I. Mustata, V. Zaroschi et al., Phys. Scr. **T 128** (2007), 157

[21] G. Sauerbrey, Z. Phys. **155** (1959), 206

[22] G. Federici, R. A. Anderl, J. N Brooks, et al., Fusion Eng. Des. **39 – 40** (1998), 445

[23] K. Dobes, V. Smejkal, T. Schäfer and F. Aumayr, Int. J. Mass Spectrom. **365 – 366** (2014), 64

[24] W. Möller and W. Eckstein, Nucl. Instrum. and Meth. B **1 – 3** (1984), 814

[25] W. Möller and B. Scherzer, J. Appl. Phys. **64** (1988), 4860

[26] W. Möller and M. Posselt, TRIDYN-FZR User Manual, FZR-317 (Institute of Ion Beam Physics and Materials Research, Forschungszentrum Rossendorf 2001).

[27] P. Sigmund, Phys. Rev. **184** (1969), 383

[28| M. Küstner, W. Eckstein, E. Hechtl and J. Roth, J. Nucl. Mat. **265** (1999), 22
[29] P. Eckerlin and A. Rabenau, Z. Anorg. Allg. Chem. **304** (1960), 218
[30] D. R. Lide (ed.), CRC Handbook of Chemistry and Physics, **Vol. 76** (1995)
[31] K. L. Wilson, R. Bastasz, R. A. Causey et al., in Atomic and Plasma-Material Interaction Data for Fusion; Supplement to Nuclear Fusion, IAEA: Vienn Austria, **Vol. 1** (1991), p. 31
[32] A. P. Zakharov, A. E. Alimov, V. Kh. Kanashenko and S L Markin, J. Nucl. Mater. **241 – 243** (1997), 52
[33] R. A. Anderl, R. A. Causey, J. W. Davis et al., J. Nucl. Mat. **273** (1999), 1
[34] C. H. Skinner, A. A. Haasz, V. K. Alimov et al., Fusion Science and Technology **54** (2008), 891
[35] G. Federici, C. H. Skinner, J. N. Brooks, et al., Nucl. Fusion **41** (2001), 1967
[36] J. Roth, E. Tsitrone, T. Loarer et al., Plasma Phys. Control. Fusion **50** (2008), 103001
[37] N. Yoshida, S. Mizusawa, R. Sakamoto and T. Muroga, J. Nucl. Mat. **874** (1996), 874
[38] A. A. Haasz and J. W. Davis, J. Nucl. Mat. **241** (1997), 1076
[39] M. Reinelt, A. Allouche, M. Oberkofler and Ch. Linsmeier, New J. Phys. **11** (2009), 043023
[40] M. Reinelt and Ch. Linsmeier, J. Nucl. Mat. **390** (2009), 568
[41] M. Oberkofler, M. Reinelt, A. Allouche, S. Lindig and Ch. Linsmeier, Phys. Scr. **T138** (2009), 014036
[42] A. Allouche, Phys. Rev. B **78** (2008), 085429
[43] V. N. Chernikov, V. K. Alimov, A. N. Markin and Q. P. Zakharov, J. Nucl. Mat. **228** (1996), 47
[44] K. Suhiyama, J. Roth, A. Anghel, et al., J. Nucl. Mat. **415** (2011), S731